Modelling the Thermal Coupling between Internal Power Semiconductor Dies of a Water-Cooled 3300V/1200A HiPak IGBT Module

Uwe DROFENIK[*], Didier COTTET[**], Andreas MÜSING[*], Jean-Marc MEYER[***] and Johann W. KOLAR[*]

[*] Power Electronic Systems Laboratory, ETH Zurich, ETH-Zentrum / ETL H13, CH-8092 Zurich, Switzerland
Phone: +41-1-632-4267, Fax: +41-1-632-1212, E-mail: **drofenik@lem.ee.ethz.ch**
[**] ABB Switzerland Ltd, Corporate Research, CH-5405 Baden-Dättwil, Switzerland
[***] ABB Switzerland Ltd, CH-5300 Turgi, Switzerland

Abstract – **Calculating the transient junction temperature of power semiconductors is important for analysing converter reliability or investigating short-term overload conditions. A dynamic thermal model, which includes the mutual thermal coupling of neighbouring dies and permits easy integration into a circuit simulator, is essential to perform such a task. In this paper, the thermal modelling procedure for a 3300V/1200A IGBT module based on numerical simulations and infrared temperature measurements is presented.**

I. INTRODUCTION

In order to analyze the reliability of a converter, knowledge of the transient junction temperature of the power semiconductors during operation is essential, especially maximum temperature values and temperature amplitudes. Transient temperature rise during short term converter overloads is also an important issue that requires dynamic thermal models for the semiconductor devices. The ability to simulate transient semiconductor temperatures with a circuit simulator will become increasingly important in a future virtual design environment, where as much of the converter as possible is designed, simulated and optimized on a computer before building a prototype.

Directly coupling of a thermal three-dimensional finite element (3D-FEM) simulation with a circuit simulation will result in inadmissible long simulation times because of the huge matrix equation that has to be solved for three-dimensional field problems at repeating time steps of the circuit simulation. Another problem that contributes to the huge computational effort is that the time constants in the circuit simulation are typically defined by switching frequencies and are therefore in the microsecond-range, while thermal time constants range from seconds for power semiconductors up to many minutes for heat sinks. A solution of this well-known problem is to extract a thermal equivalent circuit from the three-dimensional thermal model of the power module mounted onto the heat sink, which can be directly embedded into the circuit simulator.

A dynamic thermal equivalent circuit model suited for transient simulations is typically derived from the thermal step response of the power semiconductor which can be measured or numerically simulated. If the thermal step response is measured by employing a test current and measuring the semiconductor voltage drop as a function of the junction temperature, it is not necessary to open the power module or manipulate it otherwise. No exact knowledge of layer thickness, internal module design and material properties is needed. Single dies inside the power module that are connected in parallel via wire-bonding, cannot be analyzed separately. For reliability analysis it is often desirable to know internal temperatures at layer interfaces in order to evaluate the thermo-mechanical stresses at these critical points ([1], [2], [3]). If the internal geometry and the material properties of the power module are known, the thermal step responses of the individual dies can be calculated numerically via 3D-FEM based on a three-dimensional model of the power module. One big advantage of the numerical method is the accessibility of transient temperatures of all internal points of interest, especially layer interfaces and junctions.

In this paper a dynamic thermal equivalent circuit model of a power module suitable for embedding into a circuit simulator is presented. The equivalent circuit model is based on thermal step responses simulated via 3D-FEM. Therefore, it is very important to define a reliable 3D-FEM model of the power module which is the main scope of this paper. In section (II) the experimental setup for stationary measuring junction temperatures of dies inside a 3.3kV/1.2kA ABB HiPak IGBT module using infrared is described. The measured temperatures are compared to a 3D-FEM model that not only includes the power module but also the water-cooled heat sink. The measurements confirm the proposed 3D-FEM model with very good accuracy. Details of the setup of the 3D-FEM model are discussed in section (III). In section (IV) a general procedure for parameterizing a dynamic thermal equivalent circuit model that describes the thermal coupling between dies inside the power module is discussed. The procedure is based on the simulated transient thermal step responses.

Fig.1. 3300V/1200A ABB HiPak IGBT Module [4].

II. TEMPERATURE MEASUREMENTS

A. Experimental Setup

In this section temperature measurements are presented and compared to results from a 3D-FEM simulation that will be discussed in detail in section (III). As case study in this paper a water-cooled 3300V/1200A HiPak IGBT

module [4] has been chosen. The ABB HiPak IGBT modules have been presented in [5] showing excellent electrical performances, capable of withstanding extreme conditions during turn-off and short circuit operation. These modules aim at wide SOA applications operating under hard switching conditions such as traction and industrial drives. The effort undertaken to obtain such performance at semiconductor level has as a consequence also increased the demands to the package design. Extensive electrical and thermal simulations have been performed to avoid having the package as performance bottleneck. In order to guarantee high converter system reliability, transient thermal simulations are planned to be employed in future design phases. The power module, shown in **Fig.1** employs 36 internal dies, with 24 IGBTs in parallel forming the switch and 12 diodes in parallel forming the anti-parallel diode.
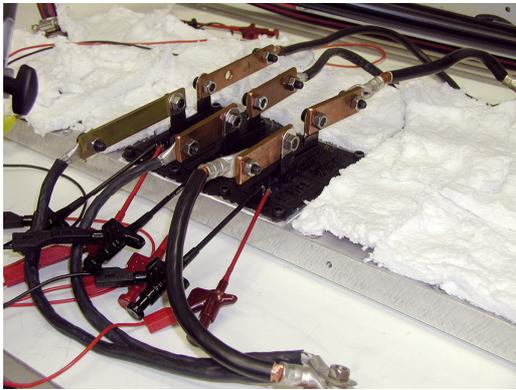
Fig.2. Experimental Setup: The housing of the power module has been removed. All surfaces are painted with a black coating for the infrared temperature measurements.

For the thermal measurements an open power module was used. The power module was attached via a thermal interface (thermal grease) to an aluminum plate employing water cooling. The water temperature at the inlet of the pipes was 20°C, the water flow through the plate was set to 23.3 liter/minute.

The camera system used to obtain the temperature pictures was a "Thermosensorik CMT 384M" infrared camera with a 284x288 pixel detector matrix and a dynamic range of 14 bits, which is sensitive in the wavelength range of λ=3-5μm. The detector pixel value is a function of temperature, spectral camera sensitivity and object emissivity. In order to improve the absolute accuracy of the thermal images, the measurements were obtained in the following way: The module surface was painted with a black coating (3M Nextel Black Paint Velvet) which has - especially in the infrared range - an emissivity close to one. This reduces measurement errors due to (metal) reflexions and varying surface properties of the power module surface. For a calibration of the absolute temperatures, the power module was heated to a spatial constant, homogeneous temperature. This results in nearly uniform reference images, containing as information only the pixel to pixel sensitivity variations, imperfections of the black coating and the reference

image temperature. The reference procedure was repeated in temperature steps of 10°C steps over the range [20°C…150°C]. Finally, the thermal images of the power module were obtained under operation. Adjusting the module measurements with an image processing software employing the reference pictures, an estimated absolute accuracy of 2°C is possible. Due to the reference image technique, the relative spatial accuracy is estimated to be even more accurate than 1°C. The experimental setup is shown in **Fig.2**.

B. Heating of Selected IGBTs and Diodes
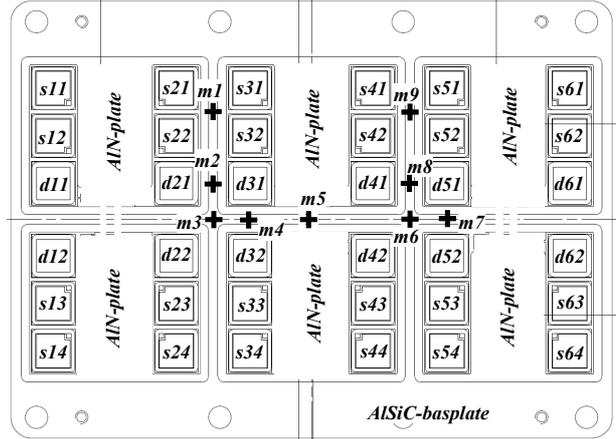
Fig.3. Internal layout of the 3300V/1200A ABB HiPak IGBT module. Here, 24 dies (labeled '*s*') are connected in parallel forming one switch, and the remaining 12 dies (labeled '*d*') connected in parallel form the anti-parallel diode. All measurements referring to '*s*'- or '*d*'-points in this paper are taken at the geometric center of the according die. Nine points (labeled '*m*') located directly on the AlSiC-base plate were chosen for additional temperature measurements.
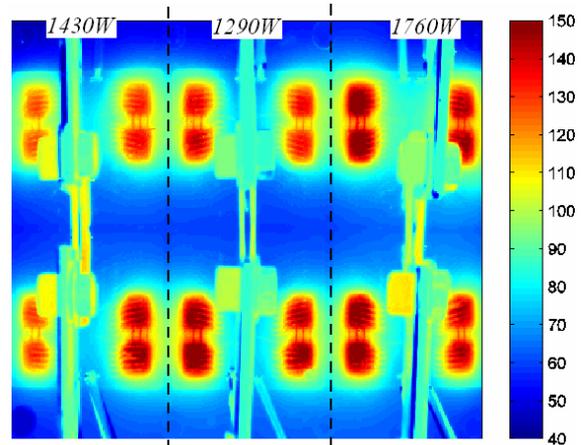
Fig.4. Stationary temperature distribution for heating all 24 IGBTs. The IGBTs *s11, s12, s13, s14, s21, s22, s23, s24* connected in parallel equally share a thermal power of 1430W (179W each), the IGBTs *s31, s32, s33, s34, s41, s42, s43, s44* connected in parallel equally share a thermal power of 1290W (161W each), the IGBTs *s51, s52, s53, s54, s61, s62, s63, s64* connected in parallel equally share a thermal power of 1760W (220W each). The total thermal power dissipated by the module is 4480W in this experiment.

Temperatures are measured at geometric centers of dies as defined in **Fig.3**. Additional points of interest are defined and labeled '*m1*', '*m2*', … '*m9*'as shown in Fig.3. By removing certain wire bond connections it was possible to

heat selected semiconductors of the power module. By measuring voltage and current, the thermal power of groups of semiconductors connected in parallel could be easily calculated. All losses are conduction losses. The measurements were taken after a stationary temperature has been reached. Stationary temperature distributions measured with the infrared camera for different configurations are given in **Fig.4**, **Fig.5**, **Fig.6** and **Fig.7**. The temperatures measured at points defined in Fig.3 are compared to 3D-FEM simulations (see section (III)) in **Tab.1** – **Tab.8**. In the tables, the heated semiconductors are highlighted.

Pts.	T[°C]	pts.	T[°C]	pts.	T[°C]	pts.	T[°C]
s11	114	s21	126	s31	128	s41	127
s12	-	s22	124	s32	129	s42	124
d11	64	d21	68	d31	66	d41	66
d12	63	d22	68	d32	66	d42	65
s13	-	s23	129	s33	129	s43	129
s14	122	s24	131	s34	134	s44	133

pts.	T[°C]	pts.	T[°C]	pts.	T[°C]	pts.	T[°C]
s51	138	s61	133	m1	92	m6	60
s52	141	s62	135	m2	66	m7	62
d51	71	d61	78	m3	60	m8	66
d52	68	d62	72	m4	60	m9	94
s53	137	s63	133	m5	60		
s54	138	s64	132				

Tab.1. Stationary temperatures measured via infrared as given in Fig.4.

Pts.	T[°C]	pts.	T[°C]	pts.	T[°C]	pts.	T[°C]
s11	115	s21	122	s31	117	s41	120
s12	116	s22	124	s32	118	s42	121
d11	58	d21	66	d31	66	d41	69
d12	59	d22	66	d32	66	d42	69
s13	117	s23	124	s33	118	s43	121
s14	116	s24	123	s34	117	s44	120

pts.	T[°C]	pts.	T[°C]	pts.	T[°C]	pts.	T[°C]
s51	141	s61	136	m1	86	m6	64
s52	143	s62	136	m2	65	m7	64
d51	72	d61	66	m3	60	m8	70
d52	71	d62	66	m4	60	m9	93
s53	143	s63	136	m5	59		
s54	142	s64	135				

Tab.2. Stationary temperatures derived via 3D-FEM simulation for the heat distribution as given in Fig.4.
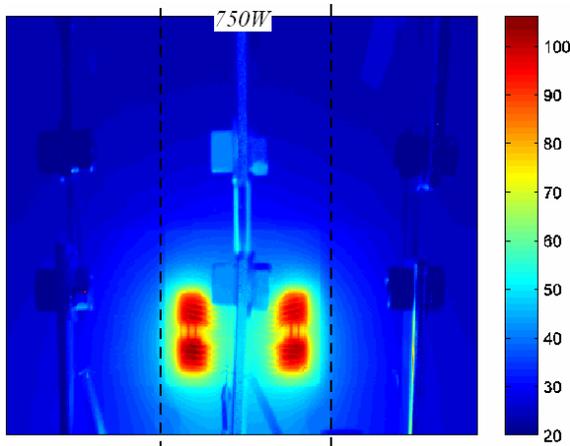
Fig.5. Stationary temperature distribution for heating four selected IGBTs. The IGBTs s33, s34, s43, s44 connected in parallel equally share a thermal power of 750W (188W each).

Pts.	T[°C]	pts.	T[°C]	pts.	T[°C]	pts.	T[°C]
s11	23	s21	24	s31	24	s41	24
s12	23	s22	25	s32	26	s42	25
d11	24	d21	26	d31	28	d41	28
d12	25	d22	32	d32	41	d42	40
s13	23	s23	36	s33	100	s43	99
s14	27	s24	38	s34	105	s44	102

pts.	T[°C]	pts.	T[°C]	pts.	T[°C]	pts.	T[°C]
s51	24	s61	23	m1	24	m6	30
s52	24	s62	22	m2	27	m7	28
d51	26	d61	24	m3	31	m8	27
d52	30	d62	25	m4	32	m9	24
s53	34	s63	25	m5	33		
s54	35	s64	26				

Tab.3. Stationary temperatures measured via infrared as given in Fig.5.

pts.	T[°C]	pts.	T[°C]	pts.	T[°C]	pts.	T[°C]
s11	21	s21	22	s31	22	s41	22
s12	21	s22	23	s32	24	s42	24
d11	22	d21	25	d31	27	d41	27
d12	23	d22	31	d32	44	d42	43
s13	23	s23	35	s33	105	s43	105
s14	23	s24	35	s34	107	s44	107

pts.	T[°C]	pts.	T[°C]	pts.	T[°C]	pts.	T[°C]
s51	22	s61	21	m1	23	m6	30
s52	23	s62	21	m2	26	m7	27
d51	25	d61	22	m3	30	m8	26
d52	31	d62	23	m4	32	m9	23
s53	35	s63	23	m5	33		
s54	35	s64	23				

Tab.4. Stationary temperatures derived via 3D-FEM simulation for the heat distribution as given in Fig.5.
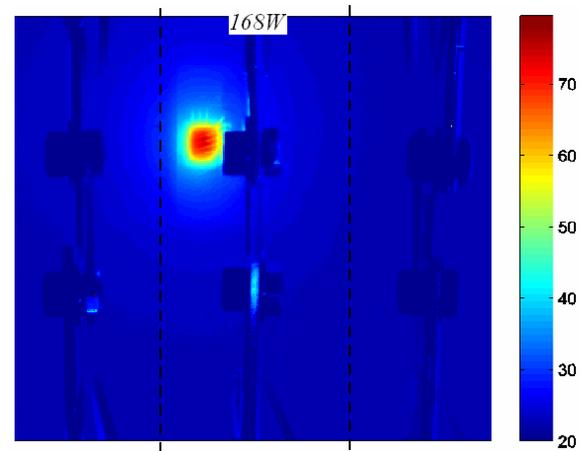
Fig.6. Stationary temperature distribution for heating one selected IGBT. The IGBT s32 dissipates a thermal power of 168W.

pts.	T[°C]	pts.	T[°C]	pts.	T[°C]	pts.	T[°C]
s11	23	s21	27	s31	32	s41	24
s12	22	s22	28	s32	73	s42	24
d11	23	d21	26	d31	31	d41	24
d12	22	d22	24	d32	24	d42	23
s13	-	s23	23	s33	23	s43	23
s14	22	s24	23	s34	23	s44	22

pts.	T[°C]	pts.	T[°C]	pts.	T[°C]	pts.	T[°C]
s51	23	s61	22	m1	33	m6	23
s52	23	s62	-	m2	29	m7	23
d51	23	d61	22	m3	25	m8	23
d52	22	d62	22	m4	26	m9	23
s53	22	s63	22	m5	25		
s54	22	s64	22				

Tab.5. Stationary temperatures measured via infrared as given in Fig.6.

pts.	T[°C]	pts.	T[°C]	pts.	T[°C]	pts.	T[°C]
s11	21	s21	25	s31	31	s41	22
s12	21	s22	26	s32	77	s42	23
d11	21	d21	25	d31	31	d41	22
d12	21	d22	22	d32	23	d42	21
s13	20	s23	21	s33	21	s43	21
s14	20	s24	21	s34	21	s44	21

pts.	T[°C]	pts.	T[°C]	pts.	T[°C]	pts.	T[°C]
s51	21	s61	20	m1	32	m6	21
s52	21	s62	20	m2	28	m7	21
d51	21	d61	20	m3	24	m8	21
d52	21	d62	20	m4	25	m9	22
s53	20	s63	20	m5	24		
s54	20	s64	20				

Tab.6. Stationary temperatures derived via 3D-FEM simulation for the heat distribution as given in Fig.6.
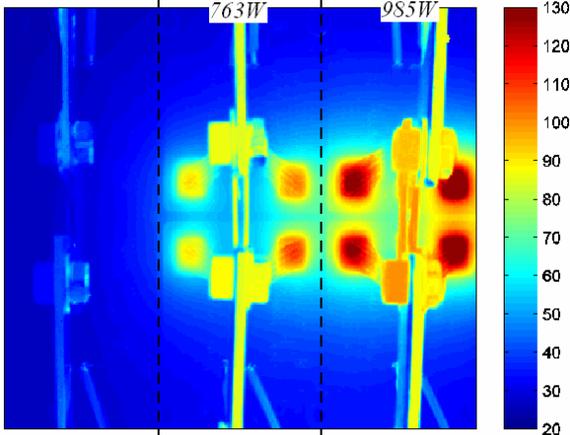
Fig.7. Stationary temperature distribution for heating eight selected diodes. The diodes *d31, d32, d41, d42* connected in parallel equally share a thermal power of 763W (191W each), the diodes *d51, d52, d61, d62* connected in parallel equally share a thermal power of 985W (246 each). The total thermal power dissipated by the module is 1748W in this experiment.

pts.	T[°C]	pts.	T[°C]	pts.	T[°C]	pts.	T[°C]
s11	25	s21	30	s31	33	s41	38
s12	25	s22	32	s32	42	s42	50
d11	26	d21	35	d31	89	d41	102
d12	26	d22	36	d32	89	d42	109
s13	30	s23	33	s33	43	s43	51
s14	26	s24	31	s34	35	s44	40

pts.	T[°C]	pts.	T[°C]	pts.	T[°C]	pts.	T[°C]
s51	40	s61	39	m1	33	m6	69
s52	55	s62	-	m2	47	m7	80
d51	128	d61	130	m3	45	m8	71
d52	122	d62	130	m4	55	m9	44
s53	54	s63	55	m5	52		
s54	40	s64	38				

Tab.7. Stationary temperatures measured via infrared as given in Fig.7.

pts.	T[°C]	pts.	T[°C]	pts.	T[°C]	pts.	T[°C]
s11	22	s21	27	s31	32	s41	38
s12	23	s22	31	s32	44	s42	54
d11	23	d21	35	d31	103	d41	117
d12	23	d22	34	d32	103	d42	117
s13	23	s23	31	s33	44	s43	54
s14	22	s24	27	s34	33	s44	38

pts.	T[°C]	pts.	T[°C]	pts.	T[°C]	pts.	T[°C]
s51	40	s61	37	m1	32	m6	81
s52	58	s62	54	m2	48	m7	88
d51	137	d61	132	m3	49	m8	81
d52	137	d62	132	m4	65	m9	46
s53	58	s63	54	m5	58		
s54	40	s64	37				

Tab.8. Stationary temperatures derived via 3D-FEM simulation for the heat distribution as given in Fig.7.

III. 3D-FEM THERMAL SIMULATION

A. General Considerations

If detailed stationary temperature distributions are available as presented in section (II), it would be not too difficult to tune material properties and/or geometries like layer thickness in a way that the 3D-FEM simulations match the measured temperatures in excellent agreement. But typically, such temperature distributions are not available due to the high experimental effort. Therefore, when building the 3D-FEM model some material properties might not be exactly known, or geometries might be simplified in order to reduce the computational effort. In this section we investigate how to generally set up a reliable 3D-FEM model for power modules, and we discuss its sensitivity concerning changes of certain parameters and/or simplifications. In this study the model always includes the water-cooled heat sink plate. For a different heat sink the model would be different, but could be easily calculated with the procedure discussed in the following. All thermal simulations are performed with the fluid-thermal 3D-FEM simulation software ICEPAK [6].

Fig.8. (a) 3D-FEM simulation of the temperature distribution at the surface of the Al-cooling plate directly below the power module for heat dissipation as defined in Fig.5. The positions of the IGBTs and diodes are shown (see Fig.3). (b) 3D-view of the Al-cooling plate with a temperature distribution according to a heat dissipation as defined in Fig.5. View from top, which is the side directly below the power module, and (c) view from bottom, which is the side in contact with the water (convective cooling).

B. Modeling the Water-Cooled Heat Sink

The heat is removed from the water-cooled aluminum plate via convection. Generally, for calculating convection, computational fluid dynamics (CFD) software is necessary. This is a kind of 3D-FEM software, where in addition to the single heat-conduction equation another four scalar equations (Navier-Stokes) describing fluid flow have to be linearized within each element. In addition to the detailed geometric layer structures within the power module resulting in a very large mesh, the

matrix equation to be solved by the CFD software becomes very large, which often causes convergence problems and numerical instabilities for such kind of problems. Another problem is that the pipes inside the cooling-plate employ very fine three-dimensional structures acting as turbulence promoters which are not defined geometrically. Therefore, the flow through these pipes cannot be simulated with acceptable accuracy.

To avoid these problems arising from convective cooling, the water-cooled plate was modeled for all 3D-FEM simulations as an aluminum plate with a defined thickness. The bottom side of this plate is defined as boundary of the 3D-FEM model by setting a homogenous heat transfer coefficient h [W/K m^{-2}] which describes with good accuracy convective heat transfer. Now, only the heat transfer equation has to be considered within each element (no CFD necessary), and the resulting matrix equation is significantly reduced, which results in comparable small simulation times, avoidance of numerical instabilities, and higher accuracy of the simulation results. The effect of convective cooling via water is still described with high accuracy.

It is important to model the cooling plate as a plate with a certain thickness [7], because the cooling plates acts as a heat spreader and contributes significantly to thermal coupling between the semiconductors inside the power module. This can be clearly seen in **Fig.8**(a) which shows the simulated temperature distribution on the surface of the cooling plate directly below the power module. If one would set the boundary condition to be of constant temperature, the simulation results would show errors, especially significant underestimation of thermal coupling. Also from the viewpoint of dynamic modeling, it is essential to define the cooling plate with the correct thickness because it represents the largest mass and, therefore, has a major effect on the thermal time constants ([7]).
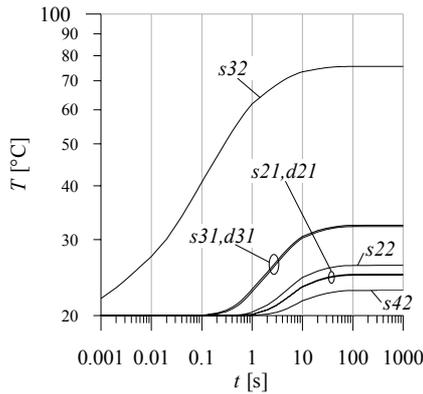
Fig.9. Thermal step responses for heating IGBT *s32*.

Thermal step responses for heating one single IGBT *s32* with 168W (see Fig.6) are shown in **Fig.9**. The temperature of the heated IGBT *s32* starts to rise after approximately 100μs. Here, the smallest time constants are defined by the masses of the silicon die and the attached solder layer. A hot spot grows underneath *s32* at the surface of the aluminum cooling plate, and after about

0.1s the cooling plate temperature underneath *s31* and *d31* (which are closest to *s32*) will start to rise as shown in Fig.9. As the hot spot grows larger, more neighbor dies will experience temperature rise. There are additional heat flow paths, e.g. horizontally through the AlN-plate (λ=180W/Km^{-1}, d=1mm) with *s32*, *s31*, *d31* and *s42* being attached to it. If this path would be dominating, there would be no significant time delay between the start of the temperature rise between, e.g., *s31* and *s42*. But as shown in Fig.9, the actual time delay between *s31* and *s42* is very large (0.1s versus 1s). Besides the aluminum cooling plate, the AlSiC base plate (see following section) is a major contributor to heat spreading and, therefore, thermal coupling of the internal semiconductors.

C. Parameters of the 3D-FEM Model

The three-dimensional structure of the power module modeled with the 3D-FEM software (ICEPAK) is shown in **Fig.10**. The interface layer between the Al-cooling plate and the AlSiC-base plate is modeled as a homogenous layer of thermal grease with thermal conductivity 1.0W/Km^{-1} and thickness 50μm. In order to simplify the 3D-model, a solder layer (λ=50W/Km^{-1} [6], d=200μm) and a copper layer (λ=380W/Km^{-1}, d=300μm) underneath the AlN-plate (λ=175W/Km^{-1}, d=1mm) are represented by a single simplified plate ("solder & copper & AlN-plate" in Fig.10) with a thickness d_{AlN}* = 1.5mm and an equivalent thermal conductivity

$$\lambda_{AlN*} = \frac{d_{AlN*}}{\sum_i d_i / \lambda_i} = \frac{d_{Solder} + d_{Cu} + d_{AlN}}{\frac{d_{Solder}}{\lambda_{Solder}} + \frac{d_{Cu}}{\lambda_{Cu}} + \frac{d_{AlN}}{\lambda_{AlN}}} = \frac{200 + 300 + 1000}{\frac{200}{50} + \frac{300}{380} + \frac{1000}{175}} \approx 140 \frac{W}{Km}$$

(1)

Also the Si-layer (λ=180W/Km^{-1}, d_{IGBT} =500μm / d_{Diode} =450μm) and the solder (λ=380W/Km^{-1}, d=70μm) underneath are represented by a simplified equivalent plate ("solder & silicon" in Fig.10) with d_{IGBT}* =570μm / d_{Diode}* =520μm and $\lambda_{IGBT} \approx \lambda_{Diode} \approx$ 130W/Km^{-1}.
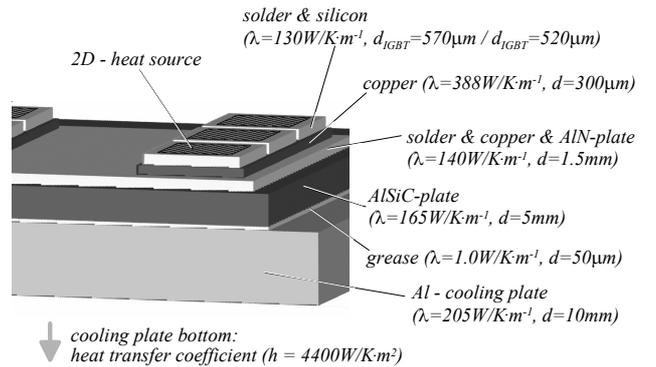
Fig.10. Structure of the layers showing the layer thicknesses and material properties as employed in the 3D-FEM simulation.

If the thermal resistance of the heat sink $R_{th,HS}$ would be given, the heat transfer coefficient h used to define the boundary condition could be simply calculated as

$$h = \left(R_{th,HS} \cdot A_{HS} \right)^{-1}$$

(2)

with heat sink surface A_{HS} (which is covered by the test-heat source for R_{th}-measurement). In this study $R_{th,HS}$ was

not known. The heat transfer coefficient was derived from temperature measurement at the power module center point *m5* in the scenario where all IGBTs are heated (Fig.4). The reason for the selection of this point is that it is located directly on the surface of the AlSiC-plate. As one can see from Fig.10, below the AlSiC-plate there is the thermal interface layer (grease) and then the Al-cooling plate. Heat flow through these three layers is much better defined than, e.g. heat flow through the semiconductor center with six additional layers involved (solder – Cu – AlN – Cu – solder – Si), where each layer might contributed small errors and/or uncertainty concerning material properties and layer geometry (thickness) which might distort and/or obfuscate the measurements. From the temperature at the AlSiC-plate center point *m5* as given in Tab.1 the heat transfer coefficient was calculated according to (2) as

$$h = \left(\frac{\Delta T_{m5}}{P_{V,total}} \cdot A_{HS, AlSiC-plate} \right)^{-1} = \left(\frac{60-20}{4480} \cdot (0.186 \cdot 0.138) \right)^{-1} = 4400 \frac{K}{Wm}$$

(3)

One key assumption for building a thermal equivalent circuit model for embedding into a circuit simulator is that the thermal material properties are temperature-independent. Strictly speaking, this assumption is violated in most cases, but for many important materials like Cu, Al or Sn the thermal conductivity can be assumed to be approximately constant over a wide temperature range as shown in **Fig.11**(a). The thermal conductivities of Si, AlN and AlSiC are shown in Fig.11(b). Over a temperature range [-50°C … +250°C] they cannot be assumed to be temperature-independent.
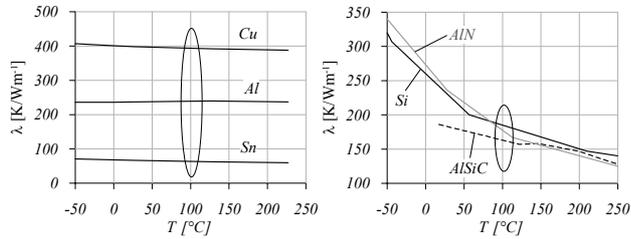
Fig.11. (a) Temperature dependency of the thermal conductivity of Cu [8], Al [8] and Sn [8]. (b) Temperature dependency of the thermal conductivity of Si [9], AlN [10] and AlSiC [11]. The ellipsoid highlights a typical thermal operating area of the power module.

Fig.11(b) shows that the thermal conductivity of AlN would be λ=200W/Km^{-1} at 75°C, but would decrease to λ=165W/Km^{-1} at 125°C. **Fig.12**(a) shows the effect of a change of the equivalent thermal conductivity of the AlN*-plate on the IGBT-temperatures for heating all IGBTs (see Fig.4). In case of a decrease of the thermal conductivity of AlN from 200W/Km^{-1} (75°C) to 165/Km^{-1} (125°C), the equivalent thermal conductivity of AlN* would decrease according to (1) from 153W/Km^{-1} (75°C) to 138W/Km^{-1} (125°C). According to Fig.12(a) this would result in a very small temperature increase of about $\Delta T \approx 2..3$°C. Because AlN shows stronger temperature-dependency than AlSiC and Si, it represents a worst-case scenario, and temperature dependencies of the material properties can be neglected in good approximation.
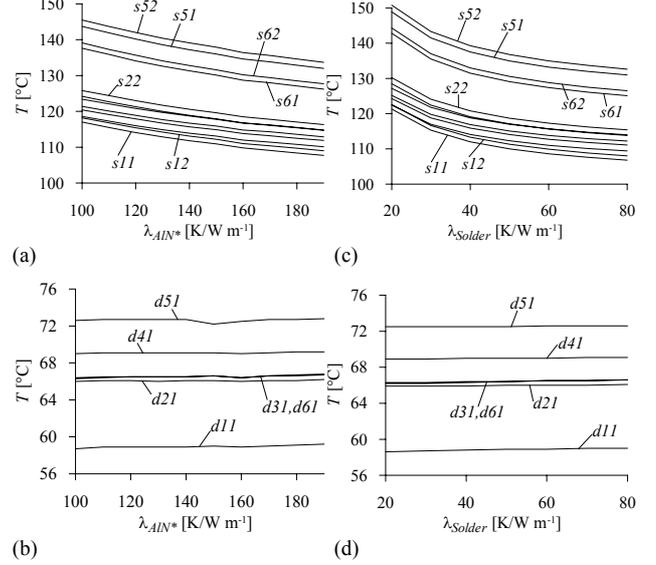
Fig.12. All IGBTs are heated as defined in Fig.4. Curves show the dependency of the temperature at certain measurement points (see Fig.3) on a variation of the thermal conductivity (a), (b) of the AlN*-plate, and (c), (d) of the solder employed between layers of the power module.

If the thermal conductivity of the solder is varying, the IGBT-temperatures change according to Fig.12(c). For an increase of λ_{Solder} from 40K/Wm^{-1} to 60W/Km^{-1}, the temperature decrease will be quite small ($\Delta T \approx 3..4$°C). The temperatures measured at the diode center points will not change in this case (Fig.12(d)). The reason is, that because only the IGBTs are heated, the temperature rise measured at the diode center points is caused not by heat flow through the diode layers (including the solder layers), but by the general rise of the temperature level at the cooling plate surface and/or AlSiC-plate due to the hot spot caused by the total thermal power of 4480W dissipated by all 24 IGBTs.

D. Modeling the Active Area of a Semiconductor

In **Fig.13** the detailed temperature distribution of IGBT *s33* is shown for heat dissipation as defined in Fig.5 (four IGBTs heated with 188W each). The mesh is defined to show at least 64 2D-elements over each two-dimensional heat source representing the active area of the chip. Therefore, the resulting mesh of the whole power module is very fine (Fig.13(a)), resulting in a total of approximately 1,000,000 elements for the whole 3D-FEM model (power module plus cooling-plate). This large number of elements would result in extremely long simulation times and a strong tendency to numerical instability in case of calculating the Navier-Stokes equations additionally to the heat conduction equation (see discussion in section (III.B)). This again shows the merits of modeling the cooling plate with a convective boundary condition instead of directly simulating the water flow.

The active area of the semiconductor is modelled by a 2D-heat source providing homogenously distributed thermal power. No wire bonds and no gate drive area are modelled. As one can see when comparing the simulation

in Fig.13(b) to the experimental measurement in Fig.13(c), the differences in the absolute temperature values are about 5°C or smaller at the selected measurement points which verifies the simple thermal semiconductor model employed in all 3D-FEM simulations. It is also interesting to note that the temperature gradient on the top surface of the silicon chip is about 25°C…30°C which is in the range of 33% with regard to the temperature difference of semiconductor to ambient $\Delta T \approx 100-20 = 80°C$.

(a)   (b)

(c)
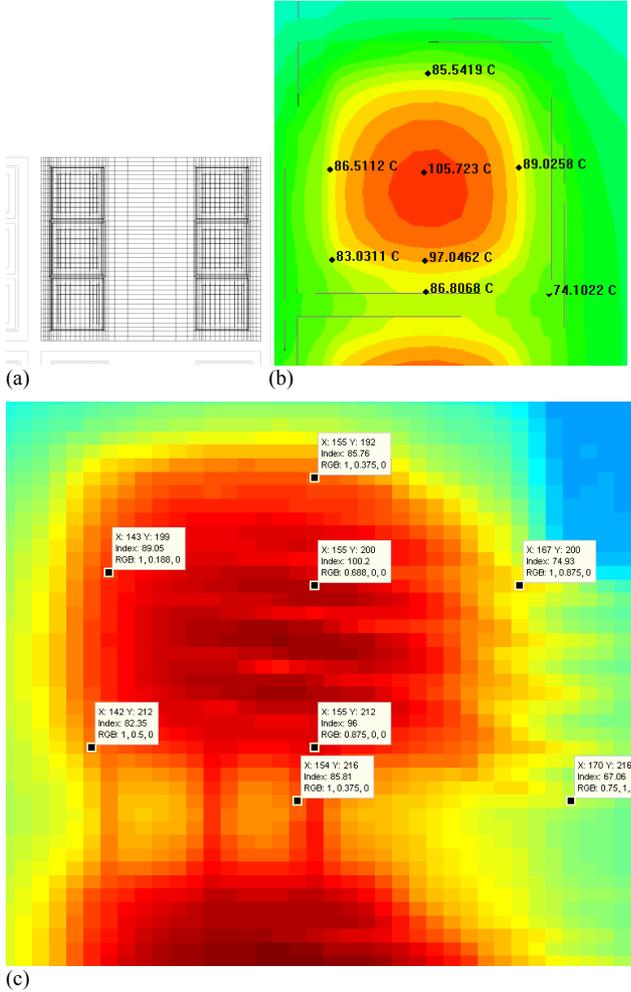
Fig.13. (a) Surface-mesh of six dies attached to an AlN-plate as employed in all 3D-FEM simulations performed in this paper. (b) 3D-FEM simulation of the temperature distribution of IGBT *s33* for heating according to Fig.5. (c) Infrared-measurement of IGBT *s33*.

IV. THERMAL MODELLING OF A POWER MODULE FOR EMBEDDING INTO A CIRCUIT SIMULATOR

A. Thermal Impedance Matrix

The thermal conduction inside a solid structure is described by the heat conduction equation

$$c_P(T) \cdot \rho \frac{\partial T}{\partial t} = \nabla \left[\lambda(T) \cdot \nabla T \right] + w(\vec{x}, t) \qquad (4)$$

with thermal capacitance c_P [Ws/(K·kg)], material density ρ [kg/m³], temperature dependent thermal conductivity λ [W/Km⁻¹], thermal power density w [W/m³], and

temperature T [K]. To create a simplified thermal model describing the dependency between the chip junction temperature and the thermal losses, two different approaches are possible. Both modeling approaches have been described in literature, and also the integration into a circuit simulation is well known (e.g. [12] - [18]).

One method is based on the Finite Difference Method (FDM) where the 3D-geometry is divided into many small volume elements, with the heat conduction equation (4) linearized within each volume element [19], [20]. The alternative modeling approach is based on an impedance matrix [21]. Here, equation (4) is assumed to be a linear differential equation (c_P, ρ, and λ not dependent on temperature) over the whole volume which is in good approximation true for many applications (see discussion in section (III.C)). Applying superposition, all thermal contributions are modeled by thermal impedance circuits that show approximately the same signal-behavior as the 3D-structure, but do not have physical meaning.

$$\begin{pmatrix} T_{junc,(1)}(t) \\ T_{junc,(2)}(t) \\ \vdots \\ T_{junc,(35)}(t) \\ T_{junc,(36)}(t) \end{pmatrix} = \begin{pmatrix} z_{1,1} & z_{1,2} & \cdots & z_{1,35} & z_{1,36} \\ z_{2,1} & z_{2,2} & \cdots & z_{2,35} & z_{2,36} \\ \vdots & \vdots & \ddots & \vdots & \vdots \\ z_{35,1} & z_{35,2} & \cdots & z_{35,35} & z_{35,36} \\ z_{36,1} & z_{36,2} & \cdots & z_{35,36} & z_{36,36} \end{pmatrix} \cdot \begin{pmatrix} p_{V,(1)}(t) \\ p_{V,(2)}(t) \\ \vdots \\ p_{V,(35)}(t) \\ p_{V,(36)}(t) \end{pmatrix} + T_{ambient}$$

(5)

Equation (5) describes the general structure of the thermal impedance matrix for a power module (plus cooling-plate) with 36 internal dies, where the transient junction temperature of each individual die is dependent on the transient thermal power dissipated by each die. The very complex and highly coupled thermal equivalent circuit resulting from this equation is shown graphically in [22], where the embedding into a circuit simulation is also discussed in more detail. The coupling occurs via elements $z_{j,k}$ that can be realized by simple single- or multistage circuits as shown in **Fig.14**.
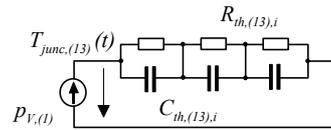
Fig.14. Thermal equivalent circuit (Foster-type) that represents one single entry $z_{1,3}$ in the matrix in (5).

In order to find the parameters $R_{th,(jk),i}$ and $C_{th,(jk),i}$ of all $z_{j,k}$ sub-circuits in (5), one has to measure or calculate the transient thermal step responses of all semiconductors of the power module. In case of the ABB HiPak IGBT module, there is the need to calculate 36 step responses and measure always the temperature rise at each of the 36 dies resulting in a total of 36×36=1296 curves. Each curve has to be represented by the according matrix entry $z_{j,k}$ in (5). Now, based on each curve the according values of $R_{th,(jk),i}$ and $C_{th,(jk),i}$ can be extracted. With higher order of the sub-circuit the number of R_{th}- and C_{th}-components increases which results in better curve fitting and higher accuracy, but also increases the computational effort when embedding the model into the circuit simulation ([22]). As an example, **Fig.15** shows all 36 thermal step responses for heating IGBT *s32* with 168W.
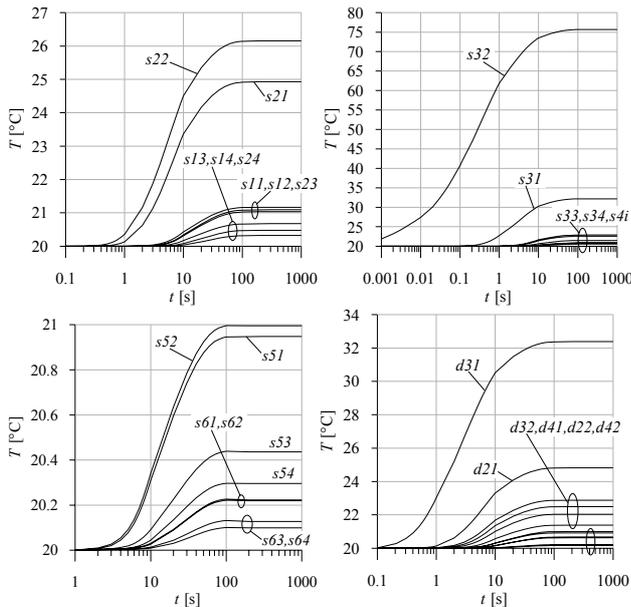
Fig.15. Transient thermal step responses from a 3D-FEM simulation. IGBT *s32* is heated by a thermal power of 168W (see Fig.6) giving transient temperatures at the centers of all 36 dies labeled s_{ij} and d_{ik}.

B. Embedding the Thermal Model into Circuit Simulator

A virtual design platform for power electronic systems is under development at PES (ETH Zurich), where the procedure of generating a thermal equivalent circuit for power modules mounted onto heat sinks as described in section (IV.A) has been implemented. One feature of this simulation platform is that complex thermally coupled models as given in (5) are built automatically from 3D-CAD models of the power module with minimum user-input necessary. This saves the user a lot of time and guarantees reliability of the model. The transient power losses, consisting of temperature-dependent conduction and switching losses, are calculated as described in [14], [19]. Junction temperatures of all 36 chips can be measured directly in the circuit simulation. For a first description of the design platform see [22].

V. CONCLUSION

A 3D-FEM model of a 3300V/1200A HiPak IGBT power module has been presented. Possible simplifications and numerical stability issues of the FEM simulation have been discussed in detail, and the sensitivity of the 3D model against parameter variations was tested. A comparison of the simulated temperature distribution with the experimental measurements obtained with an infrared camera showed a very good agreement. Therefore, the 3D-FEM model is well-suited for calculating transient thermal step responses that can be used to derive an equivalent thermal network model for embedding into a circuit simulation.

REFERENCES

[1] A. Castellazzi, M. Ciappa, W. Fichtner, G. Lourdel, M. Mermet-Guyennet, "Compact Modelling and Analysis of Power-Sharing Unbalances in IGBT-Modules Used in Traction Applications", in *Microelectronics Reliability* 46, pp. 1754 - 1759, 2006.

[2] M. Ciappa, W. Fichtner, T. Kojima, Y. Yamada, Y. Nishibe, "Extraction of Accurate Thermal Compact Models for Fast Electro-Thermal Simulation of IGBT Modules in Hybrid Electric Vehicles", in *Microelectronics Reliability* 45, pp. 1694-1699, 2005.

[3] K. Oila, M. Ciappa, N. Seliger, W. Fichtner, "Thermal Modelling, Simulation and Characterization fo a High-Temperature Converter for Automotive Applications", in *Proc. of the 10th European Conference on Power Electronics and Applications (EPE'03)*, Toulouse, France, Sept. 2 - 4, 2003.

[4] ABB Ltd, "3300V/1200A IGBT Module 5SNA 1200G330100", datasheet published at http://www.abb.com/semiconductors

[5] M. Rahimo, A. Kopta, R. Schnell, U. Schlapbach, R. Zehringer, S. Linder, "2.5kV-6.5kV Industry Standard IGBT Modules Setting a New Benchmark in SOA Capability", *Proc. of the 10th European Power Quality Conference (PCIM'04)*, Nuremberg, Germany, May 25 - 27, 2004.

[6] http://www.icepak.com/ (March 2007).

[7] U. Drofenik, J. W. Kolar, "A Thermal Model of a Forced-Cooled Heat Sink for Transient Temperature Calculations Employing a Circuit Simulator", in the *IEEJ Trans. of the Institute of Electrical Engineers of Japan*, Volume 126-D, no. 7, pp. 841-851, July 2006.

[8] J. F. Shackelford, W. Alexander, "The CRC Materials Science and Engineering Handbook", ISBN 0-8493-4276-7, CRC Press, 1992.

[9] C. J. Glassbrenner, G. A. Slack, *Phys. Rev.* **134,** 4A, A1058-A1069, 1964.

[10] G. A. Slack, R. A. Tanzilli, R. O. Pohl, J. W. Vandersande, *J. Phys. Chem. Solids* **48, 7** (1987), 641-647.

[11] M. A. Occhionero, R. W. Adams, K. P. Fennessy, "A New Substrate for Electronic Packaging: Aluminum Silicon Carbide (AlSiC) Composites," in *Proc. of the 4th Annual Portable by Design Conference,* March 24 - 27, pp 398 - 403, 1997.

[12] U. Drofenik, J. W. Kolar, "Thermal Analysis of a Multi-Chip Si/SiC-Power Module for Realization of a Bridge Leg of a 10kW Vienna Rectifier", in *Proc. of the 25th IEEE International Telecommunications Energy Conference (INTELEC'03)*, Yokohama, Japan, pp. 826 - 833, Oct. 19 - 23, 2003.

[13] U. Drofenik, J. W. Kolar, "A General Scheme for Calculating Switching- and Conduction-Losses of Power Semiconductors in Numerical Circuit Simulations of Power Electronic Systems", in *Proc. of the 2005 International Power Electronics Conf. (IPEC'05)*, Niigata, Japan, April 4 - 8, CD-ROM, ISBN: 4-88686-065-6, 2005.

[14] C.-S. Yun, "Static and Dynamic Thermal Behavior of IGBT Power Modules," *Series in Microelectronics*, Vol. 124, Dissertation ETH No. 13784, 2001.

[15] J. J. Rodriguez, Z. Parilla, M. Velez-Reyes, A. Hefner, D. Berning, J. Reichl, J. Lai, "Thermal Component Models for Electro Thermal Analysis of Multichip Power Modules," in *Proc. of the 2003 CPES Annual Seminar*, Blacksburg (VA), USA, April 27 - 29, 2003.

[16] Z. Jakopovic, V. Sunde, Z. Bencic, "From Transient Thermal Impedance Measurement to Successful Electrothermal Simulation," in *Proc. of the 10th International Power Electronics and Motion Control Conference (PEMC'02)*, Dubrovnik, Croatia, Sept. 9 - 11, CD-ROM, ISBN: 953-184-047-4, 2002.

[17] J. Chen, S. Downer, "MOSFET Loss and Junction Temperature Calculation Model in MATLAB," in *Proc. of the 10th European Power Quality Conf.*, Nuremberg, Germany, May 23 - 27, 2004.

[18] J. Z. Chen, Y. Wu, D. Borojevich, J. H. Bohn, "Integrated Electrical and Thermal Modelling and Analysis of IPEMs," in *Proc. of the 16th IEEE Applied Power Electronics Conference (APEC'01)*, Anaheim (California), USA, March 4 - 8, 2001.

[19] U. Drofenik, "Embedding Thermal Models in Power Electronic Circuit Simulation," in *Proc. of the ECPE Power Electronics Packaging Seminar,* Baden-Dättwil, Switzerland, June 7 - 8, 2004.

[20] O. Schepp, M. Lenz, "A Versatile Electrothermal Model of an Integrated Full Bridge Device Taking into Account Various Boundary Conditions," in *Proc. of the 12th IEEE Applied Power Electronics Conference (APEC'97)*, Atlanta, USA, Feb. 23 - 27, Vol. 1, pp. 185 - 190, 1997.

[21] T. Franke, G. Zaiser, J. Otto, M. Honsberg-Riedl, R. Sommer, "Current and Temperature Distribution in Multi-Chip Modules under Inverter Operation", in *Proc. of the 8th European Conference on Power Electronics and Applications (EPE'99)*, Lausanne, Switzerland, 1999.

[22] U. Drofenik, D. Cottet, A. Müsing, J.-M. Meyer, J. W. Kolar, "Computationally Efficient Integration of Complex Thermal Multi-Chip Power Module Models into Circuit Simulators", *Proc. of 4th Power Conversion Conf. (PCC'07)*, Nagoya, Japan, April 2 - 5, 2007.